

Article

A Study on the Dynamic Relationship between Landscape Information and Heat Island Intensity of Urban Growth Patterns—A Case of Five Cities in the Beijing–Tianjin–Hebei City Cluster

Jianshe Liang ¹, Yongping Bai ^{1,*}, Zuqiao Gao ², Xuedi Yang ², Lingwei Li ¹, Chunyue Zhang ¹ and Fuwei Qiao ³ ¹ College of Geography and Environmental Science, Northwest Normal University, Lanzhou 730070, China² College of Earth and Environmental Sciences, Lanzhou University, Lanzhou 730030, China³ College of Economics, Northwest Normal University, Lanzhou 730070, China

* Correspondence: baiyp@nwnu.edu.cn

Abstract: Urban heat islands (UHIs) endanger the health of urban residents. Different urban growth patterns (UGPs) have different effects on heat islands. However, the dynamic relationship between UGP landscape information and urban surface heat island intensity (SUHII) remains unclear. This study explored the dynamic relationship between SUHII and UGP landscape information through spatial regression and landscape pattern analysis using Landsat imagery and urban construction land data from five cities in the Beijing–Tianjin–Hebei urban agglomeration from 2010 to 2018. The results show that SUHII increase areas overlap with expansion patches, and the edge expansion and outlying areas show a warming effect. The influence of the edge expansion landscape area and pattern on SUHII changes is greater than the other two growth patterns. The relationship between UGPs' landscape information and SUHII changes varies among cities. The larger the city size, the stronger the influence of landscape information. Among the landscape patterns, the influence of the landscape area and pattern on SUHII change is large and the influence of landscape fragmentation is smaller. Exploring the dynamic relationship between UGP landscape information and SUHII is conducive to optimizing the spatial layout and pattern selection of urban development and providing a scientific reference for sustainable and livable urban development planning.

Keywords: urban growth patterns; landscape pattern indexes; surface urban heat island intensity; urban scale



Citation: Liang, J.; Bai, Y.; Gao, Z.; Yang, X.; Li, L.; Zhang, C.; Qiao, F. A Study on the Dynamic Relationship between Landscape Information and Heat Island Intensity of Urban Growth Patterns—A Case of Five Cities in the Beijing–Tianjin–Hebei City Cluster. *Sustainability* **2022**, *14*, 14099. <https://doi.org/10.3390/su142114099>

Academic Editors: Fernando Nardi and Laura Cavalli

Received: 14 September 2022

Accepted: 24 October 2022

Published: 28 October 2022

Publisher's Note: MDPI stays neutral with regard to jurisdictional claims in published maps and institutional affiliations.



Copyright: © 2022 by the authors. Licensee MDPI, Basel, Switzerland. This article is an open access article distributed under the terms and conditions of the Creative Commons Attribution (CC BY) license (<https://creativecommons.org/licenses/by/4.0/>).

1. Introduction

Since the reform and opening up, China's urbanization process has accelerated. From 1992 to 2015, China's urban land area increased rapidly from 1.22×10^4 km² to 7.29×10^4 km², with a nearly five-fold increase in size and an average annual growth rate of 8.10%, which is 2.5 times the global average [1]. However, the contradiction between economic development and the ecological environment has intensified during rapid urbanization, resulting in a series of negative impacts while promoting the development of the urban economy, infrastructure, and other functions [2]. The urban heat island effect is one of the more important negative impacts [3]. The risk of high temperatures due to the urban heat island effect predisposes urban residents to an increased incidence of respiratory, cardiovascular, and emotional–psychological diseases [4–6], and the hazards of the urban heat island effect are amplified in some areas along with the local background climate [7]. Therefore, the mitigation of the urban heat island effect through reasonable urban planning is an important task in building a livable city.

The measurement data of urban heat islands are divided into two categories: Air temperature data and satellite remote sensing thermal infrared band data, among which the satellite remote sensing thermal infrared band is gradually becoming an important

measurement method for urban heat islands due to its advantages of high accuracy, time continuity, and easy access to data [8,9]. The urban heat island obtained by satellite remote sensing data is called the surface urban heat island. The main influencing factor of the surface urban heat island (SUHI) effect is surface change [10], while urban growth is the main cause of surface change [11,12]. Urban growth gradually changes the surface from natural to impermeable [13,14], which converts the solar energy irradiating the surface from latent to sensible heat fluxes, making the urban surface temperature higher than that of the suburbs and generating a surface urban heat island effect [15–18]. UGPs are one of the important aspects of urban growth measurement [19,20]. It refers to the different types of growth that emerge from the differences in the location and spatial relationships of newly expanded patches based on built-up land, mainly including edge expansion, infilling, and outlying [21]. Among them, edge expansion is distributed around the original built-up area, which is bordered by the existing built-up land in the city on one side and the non-built-up land on the other side. It mainly relies on occupying the agricultural land around the city, which leads to changes in the proportion of impervious surface and vegetation cover, while more functional areas and populations are laid out within the edge type [22], which increases the anthropogenic heat emission, thus enhancing the heat island effect. Infilling is the main type of intra-urban growth, with most of its boundaries bordering already built-up urban land; it mainly occupies what were originally urban green spaces or urban restricted development areas, which can lead to a high density of population and buildings and a reduction in green space, increasing the temperature [23]. Outlying occurs at the periphery of the city and is not spatially in contact with the city's built-up land; it significantly enhances urban commuting energy consumption [24], while outlying is mostly dominated by industrial parks with a concentration of manufacturing industries, leading to an increase in surface temperature. In addition, there are differences in the warming effects of the three growth patterns due to the cold and heat island spillover effects and the different locations of the growth patches relative to the built-up urban areas, which also lead to the differences in SUHII changes they can cause. However, existing studies have mostly explored the relationship between UGPs and land surface temperature (LST) [25], and less research has been conducted on the relationship between UGPs and SUHII changes. The correlation between UGPs and SUHII is important in gaining insight into the effects of urban expansion on SUHI changes.

In addition, landscape information is usually an important influence on the formation of SUHI [26]. A large number of studies have explored the relationship between landscape configuration and SUHII by calculating the landscape pattern index [27–29]. The composition and configuration of the landscape, such as fragmentation and shape, strongly influence the formation of the SUHI [30–32]. However, few existing studies have explored the relationship with SUHII changes at the level of UGP landscape information, and the influence of UGPs as a different urban growth landscape category on SUHII is worth exploring. In addition, urban growth is more pronounced at long intervals, and SUHII changes significantly, thus making the study of SUHII dynamics even more valuable. Some scholars have explored the factors influencing SUHI dynamics [33–35], and some studies have started to simulate the future SUHI distribution [36–38]. This all proves the value of studies on SUHII dynamics, but the existing studies on UGP and SUHII are relatively inadequate in characterizing SUHII dynamics and are mostly based on static time node studies [39].

In summary, although some studies on the relationship between urban growth and SUHII dynamics have been conducted, fewer studies have explored this relationship from the perspective of UGP landscape information, and there is a lack of knowledge on how to change and plan for UGP landscape information and thus mitigate SUHII enhancement. Thus, this study investigates the dynamic relationship between UGP landscape information and SUHII changes in five cities of different scales in the Beijing–Tianjin–Hebei urban agglomeration to provide an innovative and comprehensive understanding of the dynamic relationship between UGPs and SUHII changes from the perspective of landscape informa-

tion and a scientific basis for urban planning managers in countries and regions undergoing rapid urbanization to reasonably optimize the urban layout and improve sustainable urban development. The paper is structured as follows: Section 2 gives the study area and data sources and describes the research methodology. Section 3 states the results. Section 4 gives the main conclusions and limitations.

2. Data Sources and Methods

2.1. Study Area

In this study, we selected the central urban areas of five cities in the Beijing–Tianjin–Hebei city group, namely, Beijing, Shijiazhuang, Baoding, Zhuozhou, and Gaobeidian (Figure 1). They represent different urban scales, landscape characteristics, and urbanization intensity. The urban population was calculated using the 2018 study area boundary data and Landsat population density data, and the five cities were classified into four city size classes according to the Chinese city size classification standard [40]. Beijing (with a population of 11,159,900) is a megacity, Shijiazhuang (with a population of 2,936,900) is a Type II large-sized city, Baoding (with a population of 91.63) is a medium-sized city, and Zhuozhou and Gaobeidian (with a total population of 484,600 in both cities) are Type I small cities. The study area is 7299.40 km², 1190.53 km², 916.29 km², and 378.91 km² (Zhuozhou and Gaobeidian combined), respectively. In this study, mega, large, medium, and small cities within the Beijing–Tianjin–Hebei urban agglomeration were selected for comparison based on the following considerations.

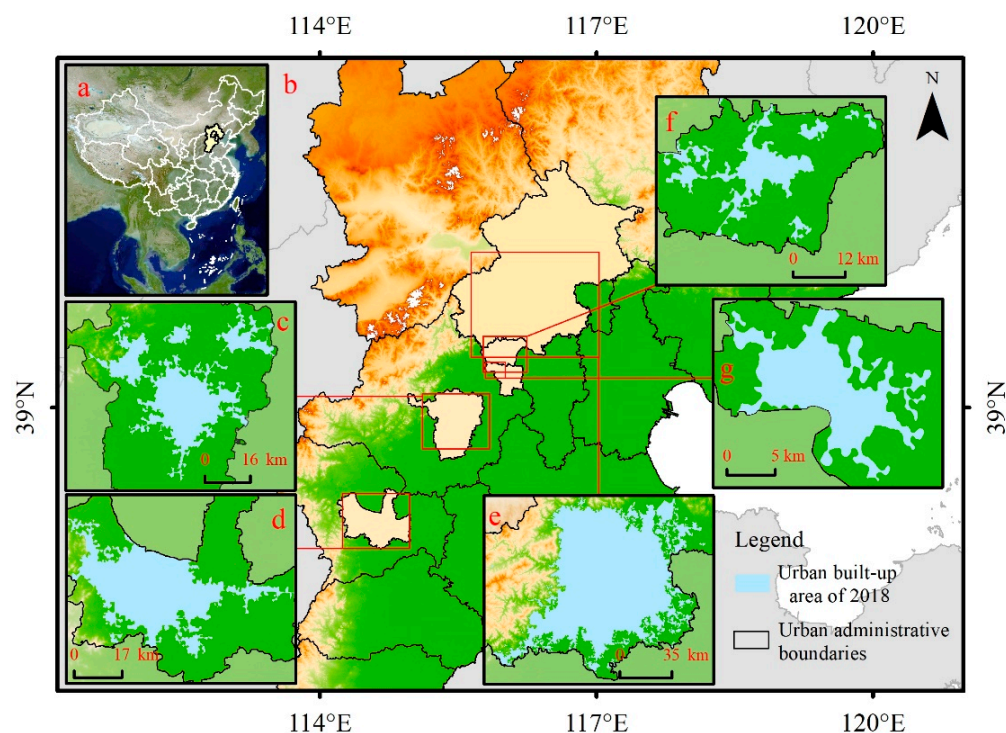


Figure 1. Study area: (a) China; (b) Beijing–Tianjin–Hebei city cluster (part of the region); (c) Baoding; (d) Shijiazhuang; (e) Beijing; (f) Zhuozhou; (g) Gaobeidian.

First, due to the differences in urban scale definition and urbanization level among different countries, to ensure that this study has reference significance for other developing countries' rapidly urbanizing regions, a comparative study of different urban scales is needed to give differentiated policies, so as many samples as possible are selected. The eastern foothills of the Taihang Mountains were chosen for the sample, where the differences in urban scale are large, instead of the coastal areas of the Beijing–Tianjin–Hebei urban agglomeration. Second, there is a typical urban class division within the Beijing–Tianjin–Hebei urban agglomeration, with a clear classification system of cities at all levels consisting of

Beijing, a megacity, as the first echelon, and Shijiazhuang and Tianjin as the second echelon. The development of the urban agglomeration has not yet reached a large contiguous belt such as that of the Yangtze River Delta, Guangdong, Hong Kong, and Macao, and the SUHI is still in faceted separation mode [41], which facilitates the study of SUHII differences among different city sizes. Third, the factors that influence urban heat islands such as climate, topography, and overall urban morphology were controlled [42–44], as the major cities within the Beijing–Tianjin–Hebei urban agglomeration selected in this study have relatively similar geomorphological conditions in terms of the difference between the highest elevation and the lowest elevation. The difference in latitude is $2^{\circ}24'$, the difference in distance from the ocean is 156.90 km, and the climatic zones all have a temperate monsoon climate. The development patterns of the main urban areas of each city are consistent, which is convenient for comparative studies. Finally, the cities selected in this study all exhibit significant heat island effects during rapid urbanization, with urban heat islands expanding rapidly outward and gradually increasing [45,46].

2.2. Data Sources and Pre-Processing

Landsat satellite images for 2010 and 2018 were downloaded from the USGS website [47] with less than 10% cloud cover. On the website of the National Meteorological Observatory of China, the start of summer in the study area is around May 21 and the start of autumn is around August 10, so this period was defined as summer in the study area. In addition, considering the low temporal resolution of the Landsat satellite in acquiring two periods of LST data, the images of the same season in adjacent years were taken as the maximum and average values in this study to eliminate the effects of extreme weather (Table 1) [48]. Radiation calibration and atmospheric correction were performed using ENVI 5.3 software during pre-processing, and the surface temperature was calculated afterwards.

Table 1. Remote sensing image data collection date.

City	Study Years	Remote Sensing Image Time
Beijing	2010	17 May 2009; 2 June 2009; 20 July 2009; 20 May 2010; 8 August 2010; 8 June 2011; 26 July 2011
	2018	23 May 2017; 10 July 2017; 13 May 2019; 29 May 2019; 14 June 2019
Shijiazhuang	2010	9 June 2009; 25 July 2009; 12 August 2009; 28 June 2010; 15 August 2010
	2018	1 July 2017; 20 July 2018; 20 May 2019
Baoding	2010	17 May 2009; 2 June 2009; 20 May 2010; 23 May 2011; 8 June 2011; 26 July 2011
	2018	23 May 2017; 8 June 2017; 10 July 2017; 20 May 2019; 29 May 2019; 14 June 2019; 30 June 2019; 23 July 2019
Zhuozhou	2010	17 May 2009; 2 June 2009; 20 May 2010; 23 May 2011; 8 June 2011; 26 July 2011
	2018	23 May 2017; 10 July 2017; 29 May 2019; 14 June 2019; 30 June 2019
Gaobeidian	2010	17 May 2009; 2 June 2009; 20 May 2010; 23 May 2011; 8 June 2011; 26 July 2011
	2018	23 May 2017; 10 July 2017; 20 May 2019; 29 May 2019; 14 June 2019; 30 June 2019;

City and built-up area boundary data were downloaded from the website [49]. ArcGIS (Version 10.5 ESRI Redlands USA) was used to extract the extent of built-up areas within the city boundaries, and then the rural settlement sites were eliminated from some of the data by comparing them with Google Earth high-resolution images so that the results were more scientific. Fragstats (Version 4.2.1 USDA USA) was used to obtain the landscape pattern index. Elements such as the landscape pattern index and SUHII difference in each study unit were calculated using ArcGIS 10.5 software for the subsequent spatial regression analysis. The specific analysis framework is shown in Figure 2

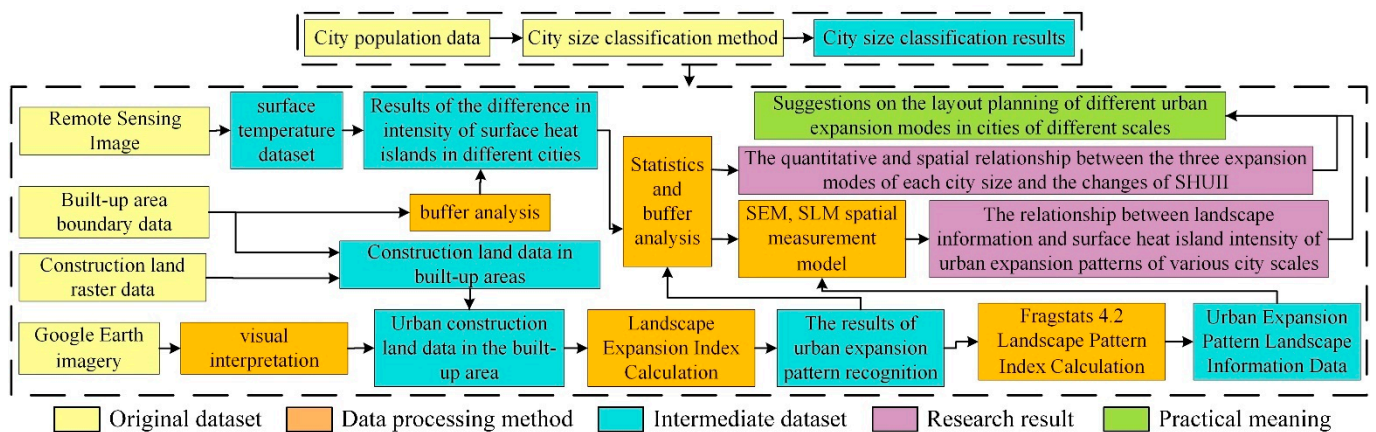


Figure 2. Analysis framework.

2.3. Methods

2.3.1. Urban Growth Index Calculation

The landscape expansion index (LEI) [50] was selected to identify the UGP:

$$LEI = \frac{L_{com}}{P_{new}} \quad (1)$$

where LEI is the landscape expansion index, L_{com} is the length of the common boundary between the new urban land and the existing urban land, and P_{new} is the perimeter of the new urban land: $LEI = 0$ for enclave type, $0 < LEI \leq 0.5$ for edge type, and $0.5 < LEI \leq 1$ for infill type.

2.3.2. LST Inversion

The transmittance and atmospheric upper radiance were obtained from the NASA website [51], and then LST inversion was performed using the radiative transfer equation method [52]. The surface-specific radiance was calculated using the hybrid image element decomposition method to classify remote sensing images into three types: Water bodies, towns, and natural surfaces.

$$\varepsilon_{surface} = 0.9625 - 0.0614F_v - 0.0461F_v^2 \quad (2)$$

$$\varepsilon_{building} = 0.9589 - 0.086F_v - 0.0671F_v^2 \quad (3)$$

where $\varepsilon_{surface}$ and $\varepsilon_{building}$ are the specific emissivities of natural surfaces and towns; F_v is the vegetation cover, determined based on the normalized difference vegetation index (NDVI).

$$F_v = \left(\frac{NDVI - NDVI_v}{NDVI_v + NDVI_s} \right)^2 \quad (4)$$

$$NDVI = \frac{NIR - Red}{NIR + Red} \quad (5)$$

where $NDVI_v = 0.70$ and $NDVI_s = 0$. When the NDVI of an image element is >0.70 , F_v takes the value of 1. When $NDVI < 0$, F_v takes the value of 0.

The equation for the brightness value of thermal infrared radiation is as follows:

$$L_\lambda = [\varepsilon \times B(T_s) + (1 - \varepsilon) \times L_\downarrow] \times \tau + L_\uparrow \quad (6)$$

$$B(T_s) = [L_\lambda - L_\uparrow - \tau(1 - \varepsilon)L_\downarrow] / \tau \times \varepsilon \quad (7)$$

where L_λ is the surface radiance; T_s is the real surface temperature in °F; $B(T_s)$ is the blackbody thermal radiation brightness introduced through Planck's law in $W/(sr \cdot m^2)$; τ is the atmospheric transmittance in the thermal infrared band; L_\uparrow is the upper atmospheric

radiation brightness in $W/(sr \cdot m^2)$; L_{\downarrow} is the ground real radiation brightness passing through the atmosphere and reaching the satellite sensor energy; and the unit is $W/(sr \cdot m^2)$. Referring to the inverse function of Planck's formula, the true surface temperature T_S in $^{\circ}C$ is derived.

$$T_S = K_2 / \ln[K_1 / B(T_S) + 1] \quad (8)$$

where K_1 and K_2 are $666.09 W (m^2 \cdot sr \cdot \mu m)^{-1}$ and $1282.7 K$ for Landsat5 TM parameters and $774.8853 W (m^2 \cdot sr \cdot \mu m)^{-1}$ and $K_2 = 1321.0789 K$ for Landsat8 OLI parameters, respectively.

In existing studies, SUHII is calculated using urban LST minus rural average LST [53]. According to a previous study [54], a 3 km buffer zone was established outside the urban boundary, the influence of mountains was removed, the zoning statistics tool of ArcGIS was used to calculate the average LST of rural areas, and then the SUHII was calculated.

$$SUHII = C_{urban} - \sum_{i=1}^n C_{rural} \quad (9)$$

where SUHII urban surface heat island effect intensity; C_{urban} is the temperature value of each image element in the urban area in $^{\circ}C$; i is the image element in the rural area in the buffer zone; n is the number of image elements in the buffer zone; and C_{rural} is the average surface temperature value in the rural area in $^{\circ}C$.

2.3.3. Landscape Pattern Index Selection

In order to determine the relationship between the SUHII difference and landscape composition and configuration, the average SUHII difference and landscape pattern index of different UGP patches were calculated separately and spatial regression analysis was performed using the Geoda (version 1.20) software. According to previous studies, the landscape pattern affecting SUHII variation is mainly landscape separation and landscape shape [55], so in this study, ENN and PROX represent the landscape separation, and FRAC and SHAPE represent the landscape shape.

2.3.4. Spatial Regression Analysis

In this study, the Moran I index was used to test whether the explanatory variables (i.e., SUHII differences) were spatially autocorrelated in the overall study area, considering that LSTs between adjacent regions may interact with each other. The results showed that the Moran I indices of the SUHII differences were all significant at the 1% level (Table 2), indicating the existence of spatial autocorrelation in the SUHII difference data and the need to introduce spatial lagged error terms or spatial lagged dependent variables in the general econometric model through the spatial weight matrix W to form a spatial econometric model. Spatial econometric models can be further classified into spatial lag models (SLMs) and spatial error models (SEMs) according to the way they deal with spatial correlation. The former assumes that spatial correlation is a consequence of the dependent variable, while the latter assumes that spatial correlation exists due to a random error term. According to the judgment criteria proposed by Anselin et al. [56] in 1996, the LMlag and LMerr were compared, and if the LMlag statistic was greater than the LMerr statistic, it indicated that the spatial correlation of the spatially lagged dependent variable dominated and SLM should be selected; otherwise, SEM should be selected.

Table 2. Moran index table of SUHII difference between expansion modes of various scales.

Scale Division	Edge Expansion	Infilling	Outlying
300 m × 300 m	0.578 ***	0.606 ***	0.581 ***
900 m × 900 m	0.433 ***	0.423 ***	0.447 ***
1500 m × 1500 m	0.338 ***	0.358 ***	0.0393 ***

Note: *** $p < 0.01$.

3. Results

3.1. Spatial and Temporal Distribution of UGPs Plaques and SUHII

From 2010 to 2018, the total urban construction land area in the study area increased by 648.14 km², which is 15.49% of the total urban area in 2010, with an overall expansion intensity of 0.0194. Along with the gradual reduction in urban size, the urban expansion area also gradually decreased. The cities (Beijing, Shijiazhuang, Baoding, Zhuozhou, and Gaobeidian) are 384.11 km², 136.09 km², 79.60 km², 27.39 km², and 20.95 km² in size, respectively. According to the results of the study, in terms of urban expansion intensity, the larger the size of the city, the lower its intensity. The expansion area of each city in 2010–2020 compared to the 2010 urban built-up area ratio was in the order of 12.02%, 26.36%, 22.35%, 36.09%, and 53.06%. The intensity of urban expansion was 0.0150, 0.0330, 0.0279, 0.0451, and 0.0663, respectively. It is worth noting that Shijiazhuang, as a large city, has a higher intensity of urban expansion compared to medium-sized cities such as Baoding. This indicates that the urban development within the Beijing–Tianjin–Hebei urban agglomeration varies greatly, and large cities such as Shijiazhuang are in a period of rapid urban development and therefore maintain a high intensity of urban expansion.

In terms of spatial distribution of expansion patches, the overall spatial distribution patterns of the three urban expansion patterns are infill, edge, and outlying from the urban center to the periphery, as shown in Figure 3. The Beijing edge type shows a significantly higher expansion in the north–south direction than in the east–west direction; the outlying type is mainly distributed in the southeast and northeast. Shijiazhuang growth patches are evenly distributed around the built-up areas, where the outlying type is more specialized, mostly in the southern area, mainly for urban infrastructure. There are more scattered blocks in Baoding city, and all of them have expanded, and the trend of expansion to the north is more obvious, mainly because the industrial land is concentrated in the north of the city. Zhuozhou and Gaobeidian have a concentrated distribution of growth patches, and most of the growth patches in the two cities are concentrated in the eastern area, as this is the distribution area of high-speed railroad stations in the two cities. The high-speed railroad stations have a significant pulling effect on the economy, so the urban expansion areas are concentrated in the eastern part.

After calculation, the surface temperature values of five cities were obtained. A comparison of the obtained surface temperature values with MODIS surface temperature products shows that the differences between them are small, and the differences in surface temperatures in the five cities are less than 2 °C. The temperature differences in the two small cities of Gaobeidian and Zhuozhou are less than 0.1 °C, indicating that the inversion accuracy is suitable for SUHI-related studies. As shown by the spatial distribution of SUHII in 2018 (Figure 4), there is a gradual decrease from the urban center to the periphery. Beijing and Shijiazhuang are all covered by heat islands, but the highest SUHII of the two cities is smaller compared to Baoding. Zhuozhou and Gaobeidian also have obvious heat island effects, but the heat island intensity is smaller compared to the larger cities. Overall, SUHII is mainly distributed in the urban built-up areas, and rivers, green areas, and some arable land obviously show the cold island phenomenon, which tentatively indicates the spatial correlation between urban built-up areas and SUHII.

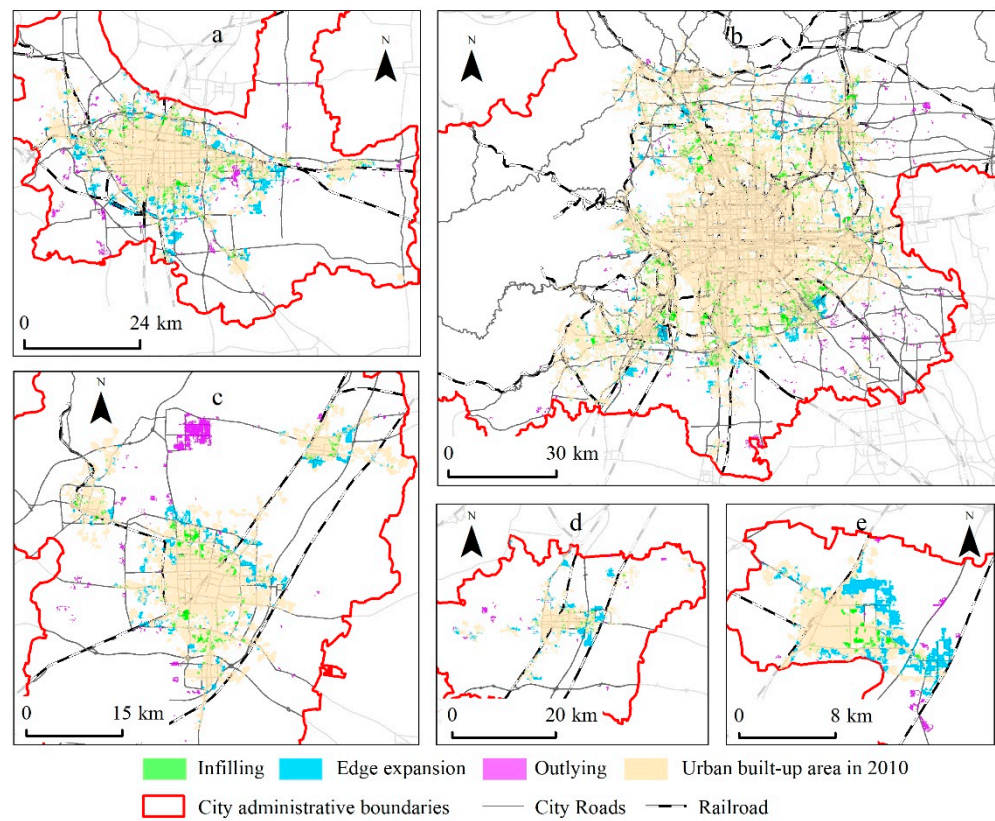


Figure 3. Spatial distribution of urban expansion patterns (2010–2018): (a) Shijiazhuang; (b) Beijing; (c) Baoding; (d) Zhuozhou; (e) Gaobeidian.

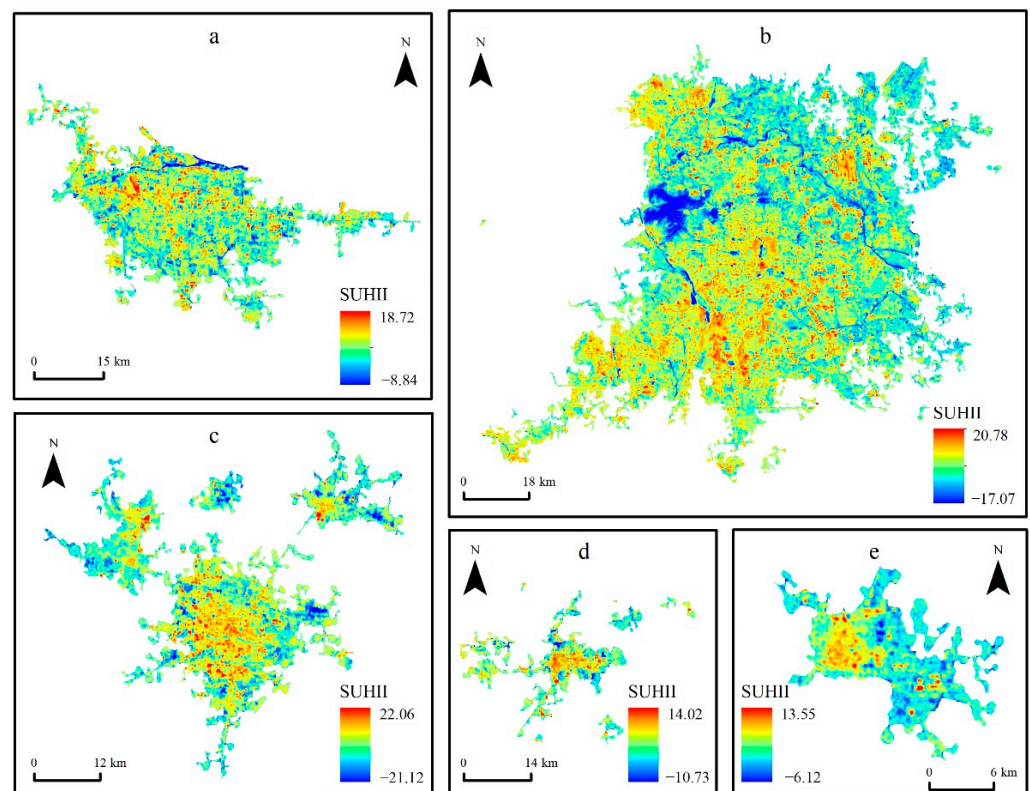


Figure 4. Distribution of SUHII by city in 2018: (a) Shijiazhuang (b) Beijing (c) Baoding (d) Zhuozhou (e) Gaobeidian.

To facilitate the dynamic study, the SUHII in 2018 was subtracted from that in 2010 to obtain the difference in SUHII over the time period under study, and the results are shown in Figure 5. Each SUHII growth area is more similar to the spatial distribution of urban growth patches. The increase in SUHII in Beijing is mainly concentrated in the north and south sides of the city, and the main increase in SUHII in Shijiazhuang is located in the east and south sides of the city. The increase in SUHII in Baoding shows a circular distribution, with an obvious increase in the enclave-type expansion of the urban area in the north of the city. The increase in SUHII in Zhuozhou and Gaobeidian on the east side is obvious. Combined with the distribution of urban growth patches in the above findings, it is shown that there is a spatial correlation between urban growth patches and SUHII growth areas. In addition, the increase in SUHII becomes larger with a larger urban scale, indicating that urban scale has a greater influence on SUHII growth. Overall, the SUHII increase area and the urban expansion area highly coincide, indicating that there is a large spatial correlation between them.

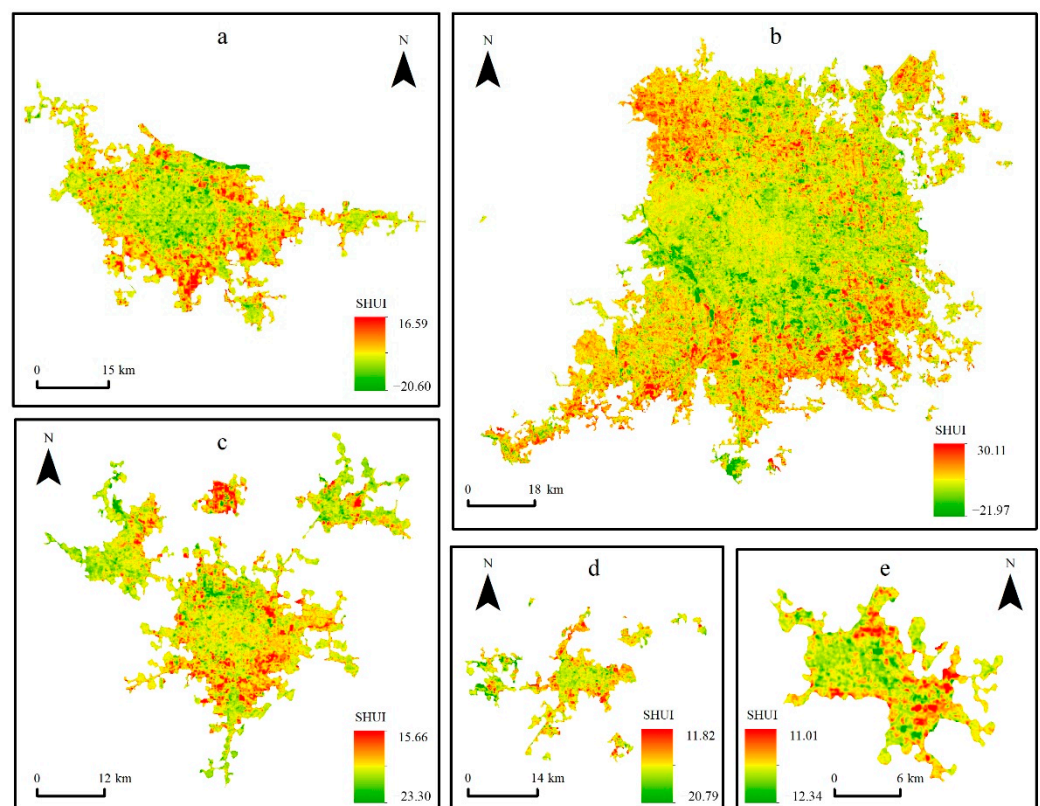


Figure 5. Distribution of SUHII differences by city (2010–2018): (a) Shijiazhuang; (b) Beijing; (c) Baoding; (d) Zhuozhou; (e) Gaobeidian.

3.2. Growth Model and SUHII Correlation

Before analyzing the relationship between UGP landscape information and SUHII, it is necessary to conduct a preliminary investigation of the relationship between UGPs and SUHII in quantitative and spatial terms. As shown in Figure 6 and Table 3, Beijing, Shijiazhuang, Baoding, and Gaobeidian have the highest SUHII changes in outlying growth patches, while the edge and infill growth patches have their own high and low SUHII changes, with the average SUHII changes being 0.534, 1.153, 0.360, and 1.861 higher than the UGPs with the smallest SUHII changes in each city, respectively. Zhuozhou has a unique change, with the largest change in SUHII in the edge expansion patches and the smallest change in the enclave, mainly due to the land use change in the outlying growth patches, which mostly consists of bare land and rural settlement land with a more obvious heat island, so the growth is slower.

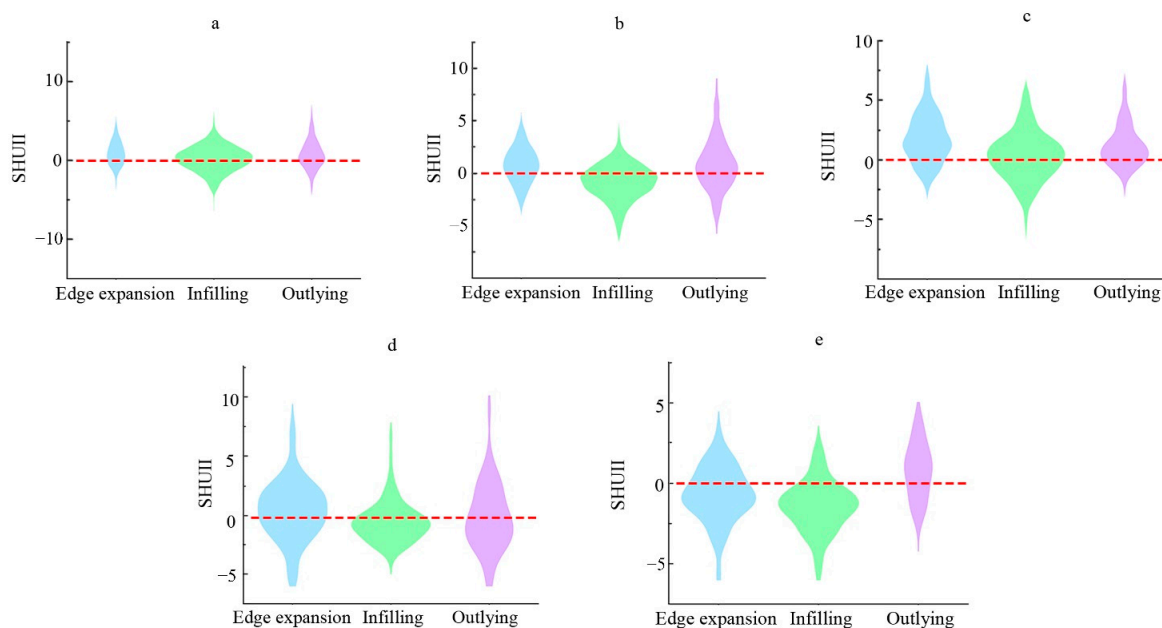


Figure 6. SUHII difference violin plot of urban expansion model (2010–2018): (a) Beijing; (b) Shijiazhuang; (c) Baoding; (d) Zhuozhou; (e) Gaobeidian.

Table 3. SUHII difference statistics of urban expansion model.

City	Edge Expansion			Infilling			Outlying		
	Median	AVG	SD	Median	AVG	SD	Median	AVG	SD
Beijing	0.355	0.261	1.821	0.293	0.263	1.821	0.568	0.795	2.047
Shijiazhuang	−0.285	−0.337	1.899	−0.331	−0.360	1.888	0.618	0.793	2.325
Baoding	0.775	0.864	2.196	0.784	0.887	2.115	0.891	1.232	1.806
Zhuozhou	−0.456	−0.219	2.069	−0.501	−0.209	2.133	−0.552	−0.289	2.704
Gaobeidian	−1.076	−1.082	1.633	−1.079	−1.079	1.598	0.850	0.782	1.689

In terms of the magnitude of change, the results of the standard deviation calculations show that all cities have the largest outlying change and the smallest infilling change.

To represent the spatial relationship between UGPs and SUHII more intuitively, regions with SUHII differences greater than zero were extracted and graded in terms of standard deviation [57]. Since there are differences in the size classes of each city, each city was graded separately to make the grading results more reasonable (Table 4). Then, the results of kernel density analysis of point of interest (POI) data and the results of the mass center analysis of built-up areas in 2010 were used to determine the city center points. Due to the different scales of cities, to ensure that the number of buffer zones is moderate for each city scale, this study established buffer zone sub-bands with a radius of 1 km and determined the area of three UGPs and SUHII sub-bands in each city within the buffer zone.

Figure 7 shows the statistical results of the buffer area analysis between different UGPs and SUHII. Overall, there is synchronization between SUHII changes and urban growth, and the area of the SUHII differential grading area becomes larger as the area of urban growth increases. In addition, there is an obvious circle structure in the urban growth pattern, and the edge shows strong synchronization with each partition of SUHII at each city scale and is more stable. With the gradual change in the urban growth pattern from the center to the periphery, the area of the SUHII differential classification also shows a large difference. Beijing's SUHII differential grading curve shows the first extreme point around the 52nd band, and this buffer zone has the largest infill area. With the gradual increase in the edge area, the area of each SUHII partition rises rapidly and finally reaches the highest point around the 45th band, where the edge area is the most, but there are also

some infill patches. After that, the edge and infill areas show a fluctuating decreasing trend along with the area of each SHUII partition. There is another small peak in the area curve of each SHUII partition between the 24th and 28th bands, where the influence of edge and infill disappears, and outlying becomes the main influence mode. Shijiazhuang also shows the same situation as Beijing, where the infill area reaches its highest value in band 35 and there is a small peak in the area of each SHUII partition. The edge area reaches its highest value in band 32 and the area of each SHUII partition in this buffer zone reaches its highest value except for the rapid warming zone and the very rapid warming zone. while near band 28, the rapid warming zone and the very rapid warming zone reach their highest values. The outlying area in this buffer zone reaches its maximum value and the edge area remains high. Near band 22, the edge area reaches its second peak, and there is also a peak period in the area of each SHUII partition. The peak area of both infill and edge in Baoding is distributed near band 26, and the area of each SHUII subzone also reaches the highest value, then the expansion area decreases, and the area of the SHUII subzone then decreases rapidly. The area of outlying reaches the highest value near band 14, and the area of each SHUII subzone also has a second peak, but the peak is smaller than the first peak at this time. Zhuozhou and Gaobeidian have less infill and outlying area due to their smaller urban size, and the edge type becomes the main influence mode for the growth of or reduction in area in each SHUII zoning district.

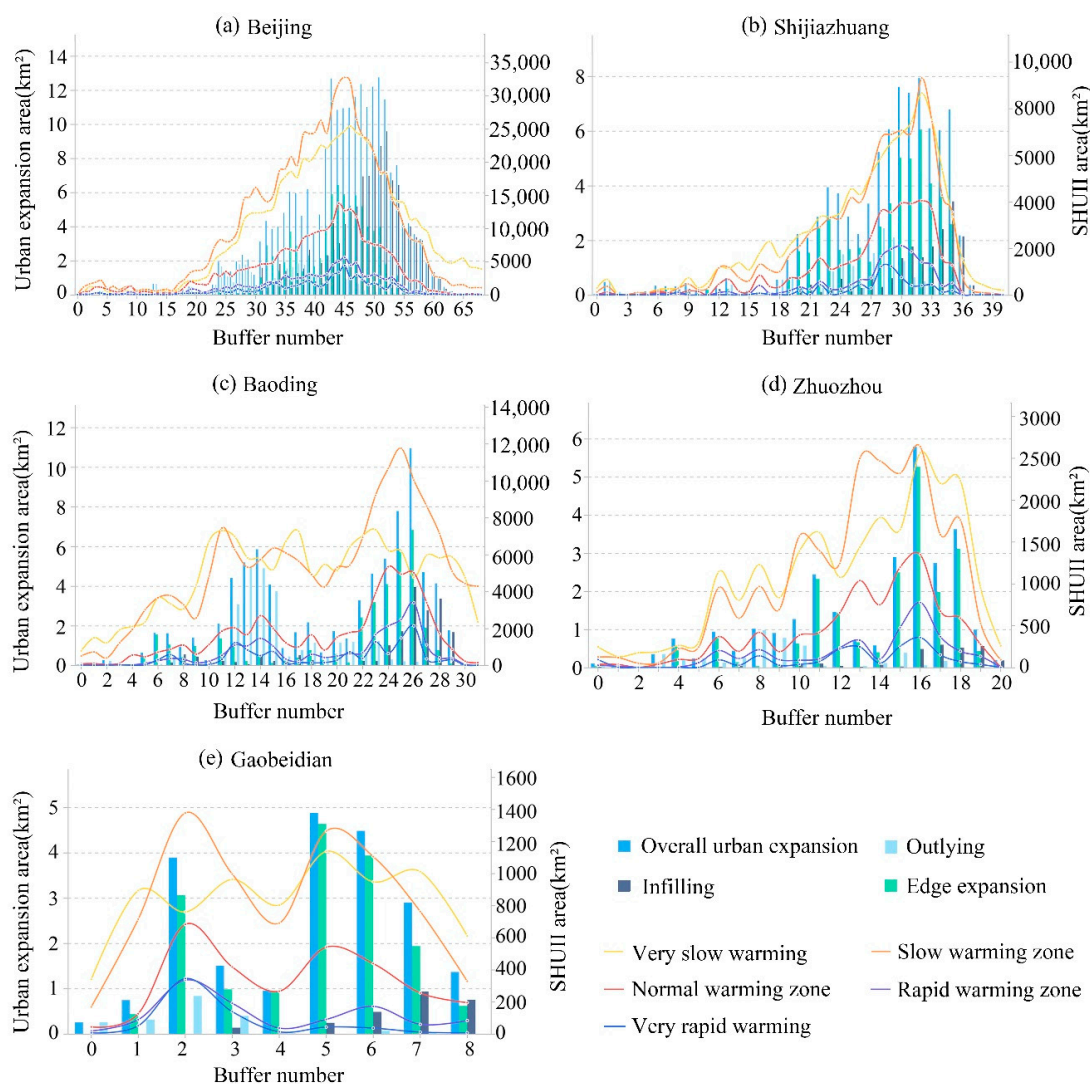


Figure 7. Analysis of urban expansion mode and SHUII graded regional buffer zone. Note: The larger the abscissa value, the closer to the city center.

Table 4. SUHII difference standard deviation level.

Graded Strength	Very Slow Warming Zone	Slow Warming Zone	Normal Warming Zone	Rapid Warming Zone	Very Rapid Warming Zone
Heat island intensity range	$SUHII < u - 1.5 \text{ std}$	$u - 1.5 \text{ std} \leq SUHII < u - 0.5 \text{ std}$	$u - 0.5 \text{ std} \leq SUHII < u + 0.5 \text{ std}$	$u + 0.5 \text{ std} \leq SUHII < u + 1.5 \text{ std}$	$SUHII \geq u + 1.5 \text{ std}$

3.3. Growth Model Landscape Information and SUHII Relationships

There are large differences in the effects of different UGP landscape areas on the changes in SUHII (Table 5). With the gradual reduction in city size, the significance gradually decreases, and Zhuozhou and Gaobeidian show an insignificant performance for all three UGP landscape areas. Each UGP landscape area shows a positive effect on SUHII. The effect of edge expansion landscape area on SUHII changes decreases with the increase in city size except for small cities, with 0.364, 0.648, and 1.698 for Beijing, Shijiazhuang, and Baoding, respectively. The infilling and outlying performed less stably, and the Beijing and Baoding outlying had the most significant effect on SUHII enhancement with correlation coefficients of 1.537 and 3.679, respectively; the Shijiazhuang edge expansion had the greatest effect on SUHII change with a correlation coefficient of 1.109.

Table 5. Regression analysis of landscape density and SUHII differences between urban expansion models.

City	Edge Expansion (R ²)	Infilling (R ²)	Outlying (R ²)
Beijing	0.364 (0.230) ***	0.527 (0.200) ***	1.537 (0.191) ***
Shijiazhuang	0.648 (0.234) ***	1.109 (0.220) ***	0.347 (0.308) ***
Baoding	1.698 (0.162) ***	0.279 (0.106) *	3.679 (0.336) ***
Zhuozhou	0.492 (0.266)	−2.680 (0.177)	2.927 (0.107)
Gaobeidian	0.056 (0.075)	−3.783 (0.041)	3.936 (0.171)

Note: *** $p < 0.01$; * $p < 0.1$.

In terms of landscape pattern, the significance and correlation coefficients of the effect of each UGP landscape separation on SUHII changes were small relative to the landscape shape. In terms of the landscape pattern, the significance and correlation coefficients of the effect of each UGP landscape separation on SUHII changes were small relative to the landscape shape. The effect of landscape separation on SUHII was mostly negative, while the landscape shape was mostly positive. The specific regression results are shown in Table 6.

The effect of landscape separation on SUHII changes was not significant for any of the urban-scale UGPs, mainly due to the large distances between sprawling patches, which was corroborated by the spatial distribution of urban growth patches in this study. The sprawling patches have less influence on each other, resulting in a larger influence of single sprawling patches compared to multiple sprawling patches. In terms of landscape shape, all exhibit a significant positive correlation except for small cities, which also indicates that the UGP single-patch influence is stronger compared to the joint effect between patches. The degree of influence of edge expansion and infilling landscape shapes on SUHII changes becomes smaller with the gradual increase in urban scale, with correlation coefficients of 4.832, 7.352, and 9.877 for Beijing, Shijiazhuang, and Baoding edge expansion and 3.891, 4.499, and 6.074 for infilling, respectively. The influence of the outlying growth pattern landscape shape index on the change of SUHII is more unstable in each city; the strongest in Baoding is 9.877 and the smallest in Shijiazhuang is 0.484, mainly because the enclave growth patches in Baoding are more concentrated and larger in area, and their shape index is also larger, which leads to more obvious warming and a greater increase in SUHII. The edge expansion has a greater impact on the landscape shape than the other two UGPs at each urban scale, which, in connection with the landscape area in the previous section, suggests that the edge type remains the UGP with the greatest impact on SUHII

changes. Both Zhuozhou and Gaobeidian have less significant landscape pattern effects. Both Zhuozhou and Gaobeidian landscape patterns have less significant effects on SUHII, due to the small size of the two cities and the fact that SUHII changes are more influenced by the local background climate, leading to this phenomenon. Another reason is that the small cities themselves have a smaller number of growth patches; the number of urban growth patches in Zhuozhou and Gaobeidian is 238 and 118, respectively, while the number of urban growth patches in Beijing, Shijiazhuang, and Baoding is 3950, 979, and 504, respectively, leading to a smaller overall sample size in the regression, and thus, the smaller cities are less significant.

Table 6. Landscape patterns and SUHII regression analysis of urban expansion models at the patch scale.

City	UGP	Landscape Separation		Landscape Shape	
		ENN (R ²)	PORX (R ²)	FRAC (R ²)	SHAPE (R ²)
Beijing	Edga expansion	−0.001 (0.222)	0.001 (0.224) ***	4.551 (0.252) ***	0.281 (0.249) ***
	Infilling	0.001 (0.184)	−0.001 (0.184)	3.632 (0.196) ***	0.259 (0.194) ***
	Outlying	−0.001 (0.171) *	0.002 (0.170)	3.949 (0.182) ***	0.341 (0.184) ***
Shijiazhuang	Edga expansion	0.001 (0.111)	−0.001 (0.121) **	6.955 (0.186) ***	0.397 (0.187) ***
	Infilling	−0.001 (0.172)	−0.004 (0.181) **	4.103 (0.189) ***	0.396 (0.193) ***
	Outlying	−0.001 (0.239)	−0.002 (0.242)	0.418 (0.237)	0.066 (0.238)
Baoding	Edga expansion	0.001 (0.066)	−0.001 (0.070)	9.353 (0.171) ***	0.524 (0.156) ***
	Infilling	0.001 (0.287)	0.007 (0.305) **	5.368 (0.305) **	0.706 (0.327) ***
	Outlying	0.001 (0.066)	−0.002 (0.069)	9.353 (0.171) ***	0.524 (0.156) ***
Zhuozhou	Edga expansion	−0.001 (0.240)	−0.001 (0.226)	5.756 (0.258) **	0.394 (0.260) **
	Infilling	0.001 (0.163) ***	−0.013 (0.069)	−0.119 (0.066)	0.090 (0.066)
	Outlying	0.001 (0.119)	0.017 (0.134)	2.695 (0.118)	−0.363 (0.127)
Gaobeidian	Edga expansion	−0.002 (0.110)	0.001 (0.108)	1.858 (0.114)	0.219 (0.128)
	Infilling	−0.001 (0.083)	−0.015 (0.079)	−1.256 (0.073)	−0.316 (0.078)
	Outlying	−0.001 (0.133)	−0.001 (0.021)	6.687 (0.112)	0.204 (0.109)

Note: *** $p < 0.01$; ** $p < 0.05$; * $p < 0.1$.

3.4. Scale Effect

Scale effects may influence the relationship between factors and SUHII changes [58–60]. In this study, to investigate the relationship between UGP landscape information and SUHII changes at different scales, the study units were set to 300 m × 300 m (10 × 10 pixels), 900 m × 900 m (30 × 30 pixels), and 1500 m × 1500 m (50 × 50 pixels) scales.

The landscape density (the result of dividing the total area of a single UGP patch in the grid by the total area of the grid) was chosen to replace the landscape area indicator to facilitate the exploration of the relationship between the change in landscape area and the difference in SUHII for the three expansion patterns at different grid scales. The regression results of both are shown in Table 7.

Overall, it is shown that the regression R² and correlation coefficient of each UGP landscape density and SUHII difference gradually become smaller as the scale increases, which indicates that the explanatory power and the degree of influence become smaller. This indicates that, despite the different city scales, the UGP has a stronger effect on SUHII changes at the 300 m scale in general. Beijing's outlying landscape density has the largest coefficient of correlation with SUHII difference, with coefficients of 17.33, 11.58, and 8.50 at each scale (300 m, 900 m, and 1500 m), followed by edge expansion, with the smallest effect of infilling and low significance at the 900 m and 1500 m scales. Shijiazhuang and Baoding edge expansion have the largest effect on the SUHII difference at all scales; Shijiazhuang has the second largest effect on outlying in general, but infilling has a larger effect than outlying at the 300 m scale, while Baoding has the second largest effect on infilling, and outlying is less significant at all scales. Zhuozhou and Gaobeidian were less significant overall, with only the edge expansion performing more significantly at all scales and the infilling and outlying not significant at all scales. In terms of urban expansion patterns, in

general, except for small cities, the edge expansion is more significant than other UGPs at all scales, and the influence of the edge expansion diminishes as the city expands. In contrast, small cities are only significant at the 300 m scale, indicating that the edge growth of small cities is generally smaller, leading to its smaller impact on SUHII at large scales. In addition, the significance of outlying and infilling is greater at the 300 m scale compared to 900 m and 1500 m for all scales except small cities, indicating that outlying and infilling have a greater impact on small scales; for the trend of change, infilling shows an unstable change with increases in the city scale, while the impact of outlying gradually increases.

Table 7. Urban landscape density and SUHII regression analysis of different scales.

City	Scale	Expansion Mode	Coefficient (R ²)	p-Value
Beijing	300	Edge expansion	11.85 (0.5316)	0.000 ***
		Infilling	9.243 (0.5002)	0.000 ***
		Outlying	17.33 (0.4857)	0.000 ***
	900	Edge expansion	3.92 (0.1868)	0.000 ***
		Infilling	1.26 (0.2931)	0.069 *
		Outlying	11.58 (0.2292)	0.000 ***
	1500	Edge expansion	2.69 (0.1652)	0.000 ***
		Infilling	0.63 (0.1483)	0.371
		Outlying	8.50 (0.2200)	0.000 ***
Shijiazhuang	300	Edge expansion	17.16 (0.5309)	0.000 ***
		Infilling	12.33 (0.4418)	0.000 ***
		Outlying	8.54 (0.5086)	0.019 **
	900	Edge expansion	4.92 (0.2122)	0.000 ***
		Infilling	−1.12 (0.2292)	0.584
		Outlying	4.23 (0.2994)	0.041 **
	1500	Edge expansion	2.75 (0.2568)	0.000 ***
		Infilling	−6.74 (0.1430)	0.001 ***
		Outlying	5.05 (0.2479)	0.006 ***
Baoding	300	Edge expansion	23.33 (0.4609)	0.000 ***
		Infilling	13.73 (0.4946)	0.003 ***
		Outlying	0.96 (0.0731)	0.847
	900	Edge expansion	6.72 (0.2626)	0.000 ***
		Infilling	6.00 (0.2787)	0.028 **
		Outlying	1.29 (0.1583)	0.156
	1500	Edge expansion	4.54 (0.2073)	0.001 ***
		Infilling	3.67 (0.2730)	0.111
		Outlying	2.10 (0.0751)	0.020 **
Zhuozhou	300	Edge expansion	17.73 (0.2328)	0.000 ***
		Infilling	5.62 (0.2701)	0.550
		Outlying	−6.42 (0.5464)	0.523
	900	Edge expansion	−0.07 (0.3680)	0.969
		Infilling	−15.69 (0.0888)	0.070 *
		Outlying	−7.99 (0.5944)	0.133
	1500	Edge expansion	1.21 (0.2195)	0.320
		Infilling	−27.79 (0.3086)	0.000 ***
		Outlying	−6.21 (0.1203)	0.270
Gaobeidian	300	Edge expansion	17.34 (0.5095)	0.000 ***
		Infilling	−14.54 (0.4441)	0.066 *
		Outlying	12.55 (0.4409)	0.252
	900	Edge expansion	1.78 (0.1471)	0.431
		Infilling	−21.47 (0.1996)	0.004 ***
		Outlying	1.75 (0.0533)	0.852
	1500	Edge expansion	0.81 (0.0240)	0.604
		Infilling	−22.17 (0.4376)	0.000 ***
		Outlying	3.59 (0.1544)	0.436

Note: * $p < 0.1$; ** $p < 0.05$; *** $p < 0.01$.

The landscape pattern indices at the grid scale were selected against the patch-scale landscape pattern indicators in the previous paper, representing the landscape area ratio (LAR), landscape fragmentation (PD, DIVISION, AI), and landscape shape (FRAC_MN, SHAPE_MN) of UGP patches.

The regression results of the difference between each UGP landscape pattern and SUHII are shown in Figure 8. In general, the significance and R² values show the same trend as the landscape density and become progressively lower with increases in city size, indicating that SUHII in megacities is more strongly influenced by the landscape pattern compared to smaller cities. Except for small cities, the significance of the three UGPs on the 300 m scale is significantly stronger than the 900 m and 1500 m scale in other scale cities, the landscape separation increases in significance compared to the patch scale, and the landscape shape becomes a negative influence. The effects of all three UGP landscape patterns on SUHII changes in small cities were not significant, indicating that changes in landscape patterns of growth patches during urban growth have little effect on SUHII.

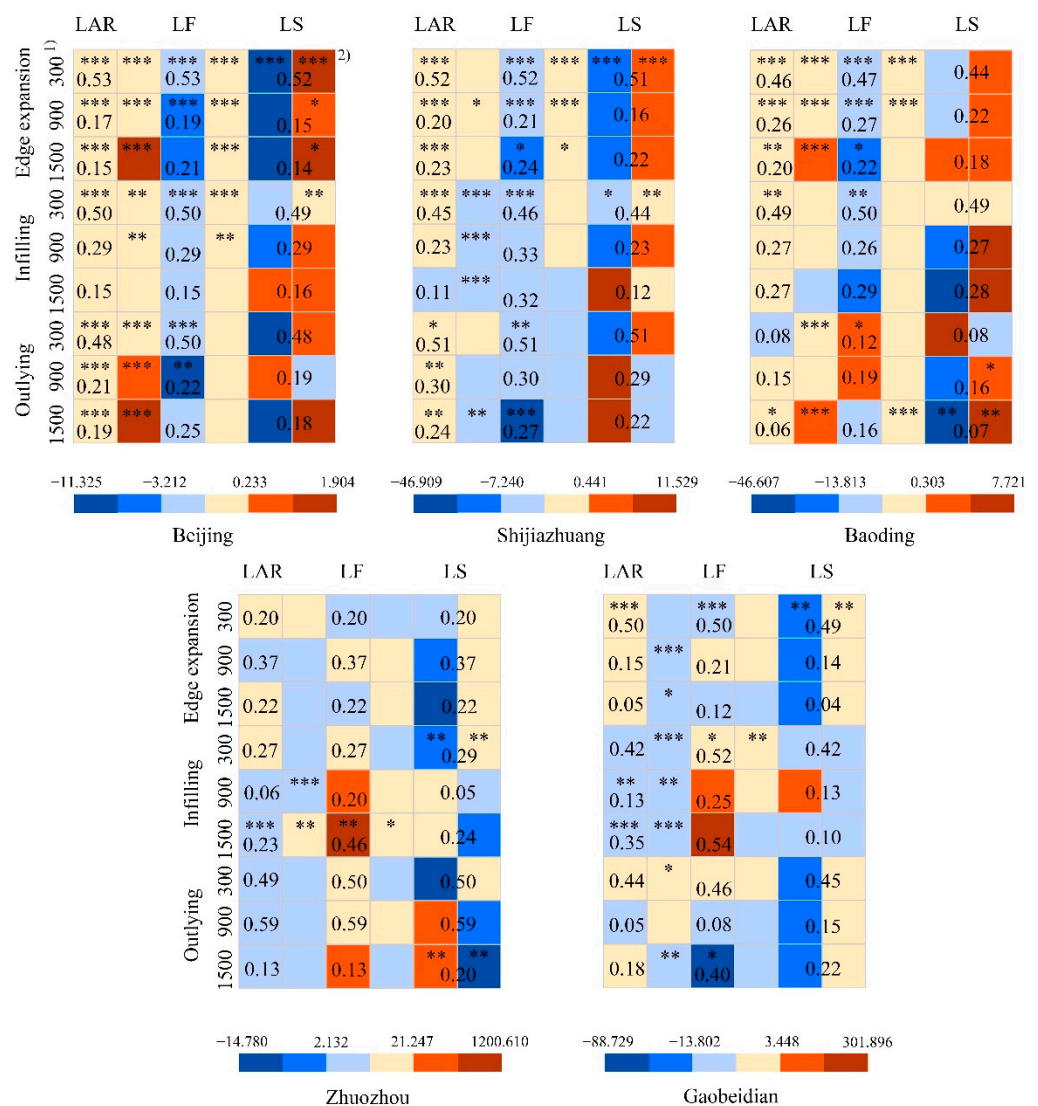


Figure 8. Landscape pattern index and SUHII regression analysis results. Notes: (1) Here the number is the grid size in meters. (2) * $p < 0.1$; ** $p < 0.05$; *** $p < 0.01$; The number is R².

The edge expansion landscape pattern decreases in significance and R² values as the city size and scale increase, and the landscape area ratio is most significant at the 300 m scale, so it becomes more important to explore the differences between city scales discussed at the 300 m scale. The edge expansion landscape area ratio had the strongest

effect on SUHII changes in Beijing and the weakest effect in Shijiazhuang, with correlation coefficients of 0.010, 0.014, and 0.018 for Beijing, Shijiazhuang, and Baoding, respectively. The effect of landscape fragmentation on the change of SUHII diminishes as the city size becomes larger. Beijing's edge-like landscape separation has the least impact compared to other cities; it has a correlation coefficient of -0.886 ; Baoding has the most impact with a correlation coefficient of -1.913 . The effect of the edge growth landscape shape on SUHII is only significant in Beijing and Shijiazhuang, which are larger cities, but not in the rest of the cities, and the effect is smaller in Beijing compared to Shijiazhuang, with correlation coefficients of -9.706 and -12.518 , respectively. The effect of the infilling landscape pattern on SUHII change was significant only for megacities and large cities, with low regularity of explanatory power differences. The correlation coefficients of the landscape area ratio in Beijing, Shijiazhuang, and Baoding at the 300 m scale were 0.008, 0.013, and 0.011, respectively. The effect of landscape separation on SUHII changes was more significant in Beijing, with a negative correlation and a correlation coefficient of -0.684 . The influence of landscape shape on SUHII changes was less significant in all city sizes and scales. The effect of the outlying landscape pattern on SUHII change only showed partial index significance in Beijing and low significance in the rest of the cities. The effect of Beijing's outlying landscape area ratio on SUHII decreases in explanatory power as the scale becomes larger, with a correlation coefficient of 0.012 at the 300 m scale. Landscape separation is more significant at the 300 m scale than at other scales, with a correlation coefficient of -1.589 . The effect of landscape shape on SUHII changes is not significant at all scales.

Overall, the explanatory power of each landscape pattern of the three UGPs in Beijing is greater than that of the other cities at the 300 m scale, while at the 900 m and 1500 m scales, it is Baoding and Shijiazhuang that have greater explanatory power, indicating that there is a significant scale effect on the influence of the three UGP landscape patterns on SUHII changes in different cities. The edge expansion landscape pattern has a significantly stronger effect on SUHII changes than the other two UGPs, while the landscape area ratio and landscape fragmentation at the grid scale have stronger effects compared to landscape shape.

At multiple scales, edge landscape information is the most influential on SUHII changes. The larger the grid scale edge landscape information scale, the smaller the R^2 and correlation coefficient, which indicates that 300 m scale edge landscape information has the strongest influence on SUHII changes. The infill landscape area varies greatly among cities at the patch scale, but its landscape pattern gradually becomes less influential with the expansion of the city scale; at the grid scale, the influence of landscape density gradually decreases with the expansion of the city scale, and the landscape pattern becomes stronger in significance, with the greatest influence at the 300 m scale on the scale difference. The influence of outlying landscape information on SUHII changes at the patch scale is not obvious among cities; however, the influence of landscape density on SUHII changes at the grid scale gradually increases with the expansion of the city scale, and the landscape pattern is strong at the 300 m scale in megacities and low in other cities, indicating that the influence of outlying landscape pattern on SUHII changes in megacities is stronger. The influence of landscape area is stronger at all scales, indicating the need to control the single patch area at both patch and grid scales. Landscape fragmentation is stronger at the grid scale than at the patch scale, suggesting that the joint effect between patches should be emphasized at the grid scale. The influence of landscape shape is stronger at the patch scale compared to the grid scale, and the correlation is the opposite, with a positive influence at the patch scale and a negative influence at the grid scale. The main reason for this phenomenon is because, under the patch scale, the roads are mostly built out first when the functional areas are laid out, and then the functional areas are laid out, which leads to a complex shape index, and the roads warm more obviously (Hendel et al., 2018) [61], presenting a positive correlation. With the small-scale grid, because it is cut by the grid, the more complex the landscape shape is, the less its SUHII increases, so it presents a negative correlation.

In summary, the process of urban growth at all scales can mitigate the enhanced urban heat island effect by controlling the landscape fragmentation between urban growth patches at the 300 m scale. At the patch scale, we should try to ensure the simultaneous construction of urban roads and urban functional areas to reduce the complexity of the patch shape. In the UGP selection, megacities should mainly use the urban stock of land for intensive development for infilling expansion. Large and medium-sized cities should gradually reduce the proportion of edge expansion, increase the proportion of infilling expansion, and pay attention to the influence of landscape patterns in the growth process. As for small cities, since they are in the early stage of urban development, edge expansion should be the main growth type in the future, but the growth process should limit the area of a single patch and gradually address the influence of landscape patterns.

4. Discussion and Conclusions

In this study, the relationship between UGP landscape information and SUHII changes in cities of different scales in the Beijing–Tianjin–Hebei urban agglomeration was investigated by controlling for other factors such as climate and topography. It was found that the relationship between different UGP landscape information and SUHII changes differed significantly among cities of various sizes. The areas of increased SUHII showed a high spatial coincidence with urban growth patches. The edge and outlying exhibited a stronger warming effect. In the landscape information correlation analysis, it was found that the patch-scale edge type was the main UGP for the increase in SUHII, and its positive effects on landscape density and landscape pattern on SUHII were larger relative to the other two UGPs in cities of all scales. At the grid scale, the 300 m scale UGP landscape information was found to have a stronger effect on SUHII changes, and the significance became stronger as the city scale increased. In addition, the landscape shape correlation is opposite to the patch scale, and the landscape area ratio at the grid scale has a positive effect on SUHII, while the landscape separation and shape index has a negative effect, indicating the existence of scale effects. The research perspective and analytical framework proposed in this study may provide new ideas for future studies related to urban growth and the thermal environment and contribute to the understanding of the complexity of urban climate.

This study also has the following limitations that could be addressed in future studies.

(1) Due to the limitation of image data resolution and processing accuracy, this study did not exclude a very small number of urban villages within the city, which affects urban renewal and partial infill plaque identification. Subsequent research can use higher-resolution remote sensing images and more accurate identification methods to refine the classification of the urban surface to improve UGP identification.

(2) City size has a large impact on the SUHI and involves many factors. In this study, due to the limitations of empirical research and the need to control for climate, topography, and overall urban morphology, the sample selection for city size was small. In future studies, high-precision algorithms can be used to simulate different city sizes under the same natural conditions and overall urban morphology in order to provide a more in-depth understanding of the relationship between the three UGPs and SUHII changes for different city sizes while controlling for other factors.

Author Contributions: J.L. was responsible for research ideas, data collection, data processing, and paper writing; Y.B. was responsible for research idea revision, research funding, and dissertation revision; Z.G. was responsible for the revision of research ideas and thesis; X.Y. was responsible for thesis revision; L.L. was responsible for thesis revision; C.Z. was responsible for thesis revision; F.Q. was responsible for thesis revision. All authors have read and agreed to the published version of the manuscript.

Funding: This research was funded by the Project of the National Natural Foundation of China (40771054), the Key R&D Program of Gansu Province, China (18YF1FA052), and the Joint project of the special scientific research fund for doctoral disciplines in colleges and universities (20106203110002).

Conflicts of Interest: The authors declare no conflict of interest.

References

- Xu, M.; He, C.; Liu, Z.; Dou, Y. How Did Urban Land Expand in China between 1992 and 2015? A Multi-Scale Landscape Analysis. *PLoS ONE* **2016**, *11*, e0154839. [[CrossRef](#)]
- Hu, J.; Yang, Y.; Zhou, Y.; Zhang, T.; Ma, Z.; Meng, X. Spatial patterns and temporal variations of footprint and intensity of surface urban heat island in 141 China cities. *Sustain. Cities Soc.* **2021**, *77*, 103585. [[CrossRef](#)]
- Wan, J.; Yong, B.; Zhou, X. Spatial and temporal analysis of the increasing effects of large-scale infrastructure construction on the surface urban heat island. *Ecotoxicol. Environ. Saf.* **2022**, *237*, 113521. [[CrossRef](#)] [[PubMed](#)]
- Rocklöv, J.; Forsberg, B.; Ebi, K.; Bellander, T. Susceptibility to mortality related to temperature and heat and cold wave duration in the population of Stockholm County, Sweden. *Glob. Health Action* **2014**, *7*, 22737. [[CrossRef](#)] [[PubMed](#)]
- Santamouris, M. Recent progress on urban overheating and heat island research. Integrated assessment of the energy, environmental, vulnerability and health impact. Synergies with the global climate change. *Energy Build.* **2020**, *207*, 109482. [[CrossRef](#)]
- Mu, H.; Li, X.; Wen, Y.; Huang, J.; Du, P.; Su, W.; Miao, S.; Geng, M. A global record of annual terrestrial Human Footprint dataset from 2000 to 2018. *Sci. Data* **2022**, *9*, 1–9. [[CrossRef](#)]
- Zhao, L.; Lee, X.; Smith, R.B.; Oleson, K. Strong contributions of local background climate to urban heat islands. *Nature* **2014**, *511*, 216–219. [[CrossRef](#)]
- Guo, G.; Wu, Z.; Chen, Y. Complex mechanisms linking land surface temperature to greenspace spatial patterns: Evidence from four southeastern Chinese cities. *Sci. Total Environ.* **2019**, *674*, 77–87. [[CrossRef](#)]
- Zhou, D.; Xiao, J.; Bonafoni, S.; Berger, C.; Deilami, K.; Zhou, Y.; Frolking, S.; Yao, R.; Qiao, Z.; Sobrino, J.A. Satellite Remote Sensing of Surface Urban Heat Islands: Progress, Challenges, and Perspectives. *Remote Sens.* **2019**, *11*, 48. [[CrossRef](#)]
- Meng, Q.; Zhang, L.; Sun, Z.; Meng, F.; Wang, L.; Sun, Y. Characterizing spatial and temporal trends of surface urban heat island effect in an urban main built-up area: A 12-year case study in Beijing, China. *Remote Sens. Environ.* **2018**, *204*, 826–837. [[CrossRef](#)]
- Wang, L.; Li, C.; Ying, Q.; Cheng, X.; Wang, X.; Li, X.; Hu, L.; Liang, L.; Yu, L.; Huang, H.; et al. China's urban expansion from 1990 to 2010 determined with satellite remote sensing. *Chin. Sci. Bull.* **2012**, *57*, 2802–2812. [[CrossRef](#)]
- Arshad, S.; Ahmad, S.R.; Abbas, S.; Asharf, A.; Siddiqui, N.A.; Islam, Z.U. Quantifying the contribution of diminishing green spaces and urban sprawl to urban heat island effect in a rapidly urbanizing metropolitan city of Pakistan. *Land Use Policy* **2021**, *113*, 105874. [[CrossRef](#)]
- Estoque, R.C.; Murayama, Y. Intensity and spatial pattern of urban land changes in the megacities of Southeast Asia. *Land Use Policy* **2015**, *48*, 213–222. [[CrossRef](#)]
- Fichera, C.R.; Modica, G.; Pollino, M. Land Cover classification and change-detection analysis using multi-temporal remote sensed imagery and landscape metrics. *Eur. J. Remote Sens.* **2012**, *45*, 1–18. [[CrossRef](#)]
- Zhao, M.; Cai, H.; Qiao, Z.; Xu, X. Influence of urban expansion on the urban heat island effect in Shanghai. *Int. J. Geogr. Inf. Sci.* **2016**, *30*, 2421–2441. [[CrossRef](#)]
- Mohajerani, A.; Bakaric, J.; Jeffrey-Bailey, T. The urban heat island effect, its causes, and mitigation, with reference to the thermal properties of asphalt concrete. *J. Environ. Manag.* **2017**, *197*, 522–538. [[CrossRef](#)]
- Tomlinson, C.J.; Chapman, L.; Thornes, J.E.; Baker, C.J. Derivation of Birmingham's summer surface urban heat island from MODIS satellite images. *Int. J. Climatol.* **2012**, *32*, 214–224. [[CrossRef](#)]
- Qiao, Z.; Tian, G.; Zhang, L.; Xu, X. Influences of Urban Expansion on Urban Heat Island in Beijing during 1989–2010. *Adv. Meteorol.* **2014**, *2014*, 187169. [[CrossRef](#)]
- Shi, Y.; Sun, X.; Zhu, X.; Li, Y.; Mei, L. Characterizing growth types and analyzing growth density distribution in response to urban growth patterns in peri-urban areas of Lianyungang City. *Landsc. Urban Plan.* **2012**, *105*, 425–433. [[CrossRef](#)]
- Jiao, L.; Mao, L.; Liu, Y. Multi-order Landscape Expansion Index: Characterizing urban expansion dynamics. *Landsc. Urban Plan.* **2015**, *137*, 30–39. [[CrossRef](#)]
- Liu, X.; Li, X.; Chen, Y.; Li, S.; Ai, B. A new landscape index for quantifying urban expansion using multi-temporal remotely sensed data. *Landsc. Ecol.* **2010**, *25*, 671–682. [[CrossRef](#)]
- He, Q.S.; He, W.S.; Song, Y.; Wu, J.Y.; Yin, C.H.; Mou, Y.C. The impact of urban growth patterns on urban vitality in newly built-up areas based on an association rules analysis using geographical 'big data'. *Land Use Policy* **2018**, *78*, 726–738. [[CrossRef](#)]
- Zhou, X.; Chen, H. Impact of urbanization-related land use land cover changes and urban morphology changes on the urban heat island phenomenon. *Sci. Total Environ.* **2018**, *635*, 1467–1476. [[CrossRef](#)]
- Kakar, K.A.; Prasad, C. Impact of urban sprawl on travel demand for public transport, private transport and walking. *Transp. Res. Procedia* **2020**, *48*, 1881–1892. [[CrossRef](#)]
- Rao, Y.; Dai, J.; Dai, D.; He, Q. Effect of urban growth pattern on land surface temperature in China: A multi-scale landscape analysis of 338 cities. *Land Use Policy* **2021**, *103*, 105314. [[CrossRef](#)]
- Yu, D.; Li, X.; Cao, Q.; Hao, R.; Qiao, J. Impacts of climate variability and landscape pattern change on evapotranspiration in a grassland landscape mosaic. *Hydrol. Process.* **2019**, *34*, 1035–1051. [[CrossRef](#)]
- Wu, Y.; Hou, H.; Wang, R.; Murayama, Y.; Wang, L.; Hu, T. Effects of landscape patterns on the morphological evolution of surface urban heat island in Hangzhou during 2000–2020. *Sustain. Cities Soc.* **2022**, *79*, 103717. [[CrossRef](#)]

28. Connors, J.P.; Galletti, C.S.; Chow, W.T.L. Landscape configuration and urban heat island effects: Assessing the relationship between landscape characteristics and land surface temperature in Phoenix, Arizona. *Landscape Ecol.* **2013**, *28*, 271–283. [CrossRef]
29. Zhou, L.; Hu, F.; Wang, B.; Wei, C.; Sun, D.; Wang, S. Relationship between urban landscape structure and land surface temperature: Spatial hierarchy and interaction effects. *Sustain. Cities Soc.* **2022**, *80*, 103795. [CrossRef]
30. Chen, Y.; Yu, S. Impacts of urban landscape patterns on urban thermal variations in Guangzhou. *China Int. J. Appl. Earth Obs. Geoinf.* **2017**, *54*, 65–71. [CrossRef]
31. Estoque, R.C.; Murayama, Y.; Myint, S.W. Effects of landscape composition and pattern on land surface temperature: An urban heat island study in the megacities of Southeast Asia. *Sci. Total Environ.* **2017**, *577*, 349–359. [CrossRef]
32. Chen, A.; Yao, X.A.; Sun, R.; Chen, L. Effect of urban green patterns on surface urban cool islands and its seasonal variations. *Urban For. Urban Green.* **2014**, *13*, 646–654. [CrossRef]
33. Liang, J.S.; Bai, Y.P.; Yang, X.D.; Gao, Z.Q.; Li, L.W.; Zhang, C.Y.; Wang, Q. Thermal Environment Evolution and Response Mechanism of Urban Sprawl Based on Multi-source Data. *Environ. Sci.* **2022**, *43*, 3365–3374. [CrossRef]
34. Chen, Y.; Shan, B.; Yu, X. Study on the spatial heterogeneity of urban heat islands and influencing factors. *Build. Environ.* **2022**, *208*, 108604. [CrossRef]
35. Sun, D.; Hu, C.; Wang, Y.; Wang, Z.; Zhang, J. Examining Spatio-Temporal Characteristics of Urban Heat Islands and Factors Driving Them in Hangzhou, China. *IEEE J. Sel. Top. Appl. Earth Obs. Remote Sens.* **2021**, *14*, 8316–8325. [CrossRef]
36. Tran, D.X.; Pla, F.; Latorre-Carmona, P.; Myint, S.W.; Caetano, M.; Kieu, H.V. Characterizing the relationship between land use land cover change and land surface temperature. *ISPRS J. Photogramm. Remote Sens.* **2017**, *124*, 119–132. [CrossRef]
37. Ouyang, X.Y.; Zhou, S.G. Hyperspectral thermal infrared TOA image simulation and preliminary applications. *Natl. Remote Sens. Bull.* **2021**, *25*, 1633–1645. [CrossRef]
38. Liu, S.; Xie, M.; Wu, R.; Wang, Y.; Li, X. Influence of the choice of geographic unit on the response of urban thermal environment: Taking Beijing as an example. *Prog. Geogr.* **2021**, *40*, 1037–1047. [CrossRef]
39. Han, R.D.; Zhang, L.; Zheng, Y.; Wang, H.; Zhang, J. Urban expansion and its ecological environmental effects in Bangkok, Thailand. *Acta Ecol. Sin.* **2017**, *37*, 6322–6334.
40. CGPRC (Central Government of the People’s Republic of China). Circular of the State Council on Adjusting the Criteria for the Classification of City Sizes. 2014. Available online: http://www.gov.cn/zhengce/content/2014-11/20/content_9225.htm (accessed on 11 May 2022).
41. Hou, L.; Yue, W.; Liu, X. Spatiotemporal patterns and drivers of summer heat island in Beijing-Tianjin-Hebei Urban Agglomeration, China. *IEEE J. Sel. Top. Appl. Earth Obs. Remote Sens.* **2021**, *14*, 7516–7527. [CrossRef]
42. Sun, R.; Lü, Y.; Yang, X.; Chen, L. Understanding the variability of urban heat islands from local background climate and urbanization. *J. Clean. Prod.* **2018**, *208*, 743–752. [CrossRef]
43. Liu, Y.; Li, Q.; Yang, L.; Mu, K.; Zhang, M.; Liu, J. Urban heat island effects of various urban morphologies under regional climate conditions. *Sci. Total Environ.* **2020**, *743*, 140589. [CrossRef]
44. Liu, X.; Ming, Y.; Liu, Y.; Yue, W.; Han, G. Influences of landform and urban form factors on urban heat island: Comparative case study between Chengdu and Chongqing. *Sci. Total Environ.* **2022**, *820*, 153395. [CrossRef]
45. Chen, M.; Zhou, Y.; Hu, M.; Zhou, Y. Influence of Urban Scale and Urban Expansion on the Urban Heat Island Effect in Metropolitan Areas: Case Study of Beijing-Tianjin-Hebei Urban Agglomeration. *Remote Sens.* **2020**, *12*, 3491. [CrossRef]
46. Zhao, G.; Dong, J.; Liu, J.; Zhai, J.; Cui, Y.; He, T.; Xiao, X. Different Patterns in Daytime and Nighttime Thermal Effects of Urbanization in Beijing-Tianjin-Hebei Urban Agglomeration. *Remote Sens.* **2017**, *9*, 121. [CrossRef]
47. USGS Official Website. Available online: <http://earthexplorer.usgs.gov/> (accessed on 25 May 2022).
48. Simwanda, M.; Ranagalage, M.; Estoque, R.C.; Murayama, Y. Spatial Analysis of Surface Urban Heat Islands in Four Rapidly Growing African Cities. *Remote Sens.* **2019**, *11*, 1645. [CrossRef]
49. Global Land Cover. Available online: <http://data.ess.tsinghua.edu.cn/> (accessed on 30 May 2021).
50. Liu, X.; Ma, L.; Li, X.; Ai, B.; Li, S.; He, Z. Simulating urban growth by integrating landscape expansion index (LEI) and cellular automata. *Int. J. Geogr. Inf. Sci.* **2013**, *28*, 148–163. [CrossRef]
51. Atmospheric Correction Parameter Calculator. Available online: <http://atmcorr.gsfc.nasa.gov/> (accessed on 26 May 2021).
52. Jiménez-Muñoz, J.C.; Sobrino, J.A.; Skoković, D.; Mattar, C.; Cristóbal, J. Land Surface Temperature Retrieval Methods from Landsat-8 Thermal Infrared Sensor Data. *IEEE Geosci. Remote Sens. Lett.* **2014**, *11*, 1840–1843. [CrossRef]
53. Peng, S.; Piao, S.; Ciais, P.; Friedlingstein, P.; Ottle, C.; Bréon, F.-M.; Nan, H.; Zhou, L.; Myneni, R.B. Surface Urban Heat Island Across 419 Global Big Cities. *Environ. Sci. Technol.* **2011**, *46*, 696–703. [CrossRef]
54. Yao, R.; Wang, L.; Huang, X.; Niu, Y.; Chen, Y.; Niu, Z. The influence of different data and method on estimating the surface urban heat island intensity. *Ecol. Indic.* **2018**, *89*, 45–55. [CrossRef]
55. Chen, A.; Sun, R.; Chen, L. Studies on urban heat island from a landscape pattern view: A review. *Acta Ecol. Sin.* **2012**, *32*, 4553–4565. [CrossRef]
56. Anselin, L.; Bera, A.K.; Florax, R.; Yoon, M.J. Simple diagnostic tests for spatial dependence. *Reg. Sci. Urban Econ.* **1996**, *26*, 77–104. [CrossRef]
57. Ying, X.; Fang, Z. Thermal environment effects of urban human settlements and influencing factors based on multi-source data: A case study of Changsha city. *Acta Geogr. Sin.* **2020**, *75*, 2443–2458. [CrossRef]

58. Kang, S.; Lee, D.; Park, J.; Jung, J. Exploring Urban Forms Vulnerable to Urban Heat Islands: A Multiscale Analysis. *Sustainability* **2022**, *14*, 3603. [[CrossRef](#)]
59. Ziter, C.D.; Pedersen, E.J.; Kucharik, C.J.; Turner, M.G. Scale-dependent interactions between tree canopy cover and impervious surfaces reduce daytime urban heat during summer. *Proc. Natl. Acad. Sci. USA* **2019**, *116*, 7575–7580. [[CrossRef](#)] [[PubMed](#)]
60. Su, W.X.; Zhang, L.K.; Chang, Q. Coupling analysis of urban thermal environment and landscape characteristics based on optimal granularity. *China Environ. Sci.* **2022**, *42*, 954–961. [[CrossRef](#)]
61. Hendel, M.; Parison, S.; Grados, A.; Royon, L. Which pavement structures are best suited to limiting the UHI effect? A laboratory-scale study of Parisian pavement structures. *Build. Environ.* **2018**, *144*, 216–229. [[CrossRef](#)]